Iterative sorting of apical and basolateral cargo in Madin–Darby canine kidney cells

Aleksandr Treyer[a], Mario Pujato[b,c], Ximo Pechuan[b], and Anne Müsch[a,*]
[a]Department of Developmental and Molecular Biology and [b]Department of Systems and Computational Biology, Albert Einstein College of Medicine, Bronx, NY 10461; [c]Center for Autoimmune Genomics and Etiology, Cincinnati Children's Hospital Medical Center, Cincinnati, OH 45229

ABSTRACT **For several decades, the *trans*-Golgi network (TGN) was considered the most distal stop and hence the ultimate protein-sorting station for distinct apical and basolateral transport carriers that reach their respective surface domains in the direct trafficking pathway. However, recent reports of apical and basolateral cargoes traversing post-Golgi compartments accessible to endocytic ligands before their arrival at the cell surface and the post-TGN breakup of large pleomorphic membrane fragments that exit the Golgi region toward the surface raised the possibility that compartments distal to the TGN mediate or contribute to biosynthetic sorting. Here we describe the development of a novel assay that quantitatively distinguishes different cargo pairs by their degree of colocalization at the TGN and by the evolution of colocalization during their TGN-to-surface transport. Keys to the high resolution of our approach are 1) conversion of perinuclear organelle clustering into a two-dimensional microsomal spread and 2) identification of TGN and post-TGN cargo without the need for a TGN marker that universally cosegregates with all cargo. Using our assay, we provide the first evidence that apical NTRp75 and basolateral VSVG in Madin–Darby canine kidney cells still undergo progressive sorting after they exit the TGN toward the cell surface.**

Monitoring Editor
Patrick J. Brennwald
University of North Carolina

Received: Feb 10, 2016
Revised: May 17, 2016
Accepted: May 19, 2016

INTRODUCTION

Newly synthesized plasma membrane, secretory, and lysosomal proteins all enter the extracytoplasmic space with their translocation into the endoplasmic reticulum (ER) membrane/lumen. They segregate along their passage through the secretory pathway to incorporate into distinct membranous carriers that deliver the cargoes by fusing with their respective destination membrane. Epithelial cells further sort membrane and secretory proteins into distinct carriers destined for either the apical or the basolateral membrane domain. The textbook idea for the past 30 yr has been that sorting of apical, basolateral, and lysosomal proteins occurs at the *trans*-Golgi network (TGN; Griffiths and Simons, 1986). This assumption was derived from two key observations: 1) immuno–electron microscopy (EM) showed apical and basolateral cargoes still mixed throughout the cisternae of the Golgi stack (Rindler *et al.*, 1984), and 2) the finding, confirmed in many studies, that when cells were incubated at 20°C, lysosomal hydrolases and secretory and plasma membrane cargo reversibly accumulated at the *trans* side of the Golgi apparatus and, after reversal of the temperature block, were released in distinct transport carriers toward distinct cell surface domains and prelysosomal compartments, respectively (Rindler *et al.*, 1985; Wandinger-Ness *et al.*, 1990; Keller *et al.*, 2001). Thin section transmission immuno-electron microscopy (immuno-EM) after cargo accumulation at 20°C furthermore revealed the TGN to be a tubular compartment with many budding coated structures. These buds were believed to give rise to different types of coated vesicles (Wehland *et al.*, 1982), which represents the only well-understood mechanism that coordinates protein sorting with transport carrier formation.

Two paradigm shifts in the past decade, however, call for a reevaluation of the TGN as the primary sorting station for apical

This article was published online ahead of print in MBoC in Press (http://www.molbiolcell.org/cgi/doi/10.1091/mbc.E16-02-0096) on May 25, 2016.

*Address correspondence to: Anne Müsch (anne.muesch@einstein.yu.edu).

Abbreviations used: CAD, conditional aggregation domain; CCI, corrected correlation index; CRE, common recycling endosome; DPPIV, dipeptidyl peptidase IV; ER, endoplasmic reticulum; FP, fluorescent protein; GFP, green fluorescent protein; hTfR, human transferrin receptor; mBFP, monomeric blue fluorescent protein; MDCK, Madin–Darby canine kidney cells, mRFP, monomeric red fluorescent protein; NTRp75, neurotrophin receptor p75(NTR); ST, sialyltransferase; Tfn, transferrin; TGN, *trans*-Golgi network; VSVG, vesicular stomatitis virus protein G; VSVG-SP, temperature-sensitive ts045 mutant of VSVG containing a short polypeptide linker to separate a potential fusion moiety from the VSVG sequence.

© 2016 Treyer *et al.* This article is distributed by The American Society for Cell Biology under license from the author(s). Two months after publication it is available to the public under an Attribution–Noncommercial–Share Alike 3.0 Unported Creative Commons License (http://creativecommons.org/licenses/by-nc-sa/3.0).
"ASCB®," "The American Society for Cell Biology®," and "Molecular Biology of the Cell®" are registered trademarks of The American Society for Cell Biology.

and basolateral proteins in the biosynthetic pathway. First, live-cell imaging coupled with correlative EM revealed that exocytic cargo leaves the Golgi not in coated vesicles but in large pleomorphic structures that range in size from several hundred nanometers to several micrometers, which break up into smaller carriers as they move away from the Golgi (Polishchuk *et al.*, 2000). This tubular mode of Golgi exit has been observed for proteins with apical and basolateral sorting signals in polarized and nonpolarized cell types, but how cargo sorting is related to tubule formation and their fragmentation is not understood (De Matteis and Luini 2008). Thus apical-basolateral protein sorting could occur before tubule formation at the Golgi, resulting in distinct apical and basolateral structures that exit the Golgi, as assumed for the coated-vesicle hypothesis. Alternatively, protein sorting could occur after tubules leave the Golgi and coincide with their breakup into smaller carriers.

The second paradigm-shifting discovery was that the TGN is not in fact the most distal endomembrane compartment that exocytic cargoes traverse before reaching the cell surface. Membrane and secretory proteins were shown to pass through various endosomal compartments after the release of the 20°C block but before they arrive at the cell surface (Folsch *et al.*, 2009). Because endosomes execute protein sorting in the recycling pathways, it has been postulated that endosomal passage is part of an iterative process of protein sorting in the exocytic route. Evidence for this hypothesis, however, is controversial (Keller *et al.*, 2001; Ang *et al.*, 2004; Cresawn *et al.*, 2007). In studies that analyzed both apical and basolateral cargoes, functional ablation of endosomal compartments that inhibited basolateral exocytosis had no effect on apical cargoes and vice versa—a scenario more in line with independent post-Golgi itineraries for apical and basolateral proteins than with their sorting in common endosomes (Cresawn *et al.*, 2007). In a different approach, an apical version of vesicular stomatitis virus glycoprotein G (VSVG) was transiently affinity isolated with transferrin-positive endosomes to the same extent as basolateral VSVG during each cargo's separate exocytic itinerary (Ang *et al.*, 2004).

Determining the relative contributions of the TGN and post-Golgi tubular carriers and endosomal compartments to protein sorting requires direct visualization of apical and basolateral cargo distribution within the TGN and within post-TGN membrane compartments during their simultaneous passage through the secretory pathway. This presents two major challenges. First, the axial resolution achievable by light microscopy is close to the thickness of the entire Golgi stack, which is ~290 nm (Ladinsky *et al.*, 1999; 100–300 nm in three-dimensional [3D] superresolution techniques such as structured illumination microscopy). In addition, the microtubule-organizing center that positions the Golgi in the perinuclear region directs many endosomal populations there as well. In particular, the common recycling endosome (CRE), which sorts apical and basolateral proteins for recycling in the endocytic route (Odorizzi *et al.*, 1996; Wang *et al.*, 2001; Thompson *et al.*, 2007), closely abuts the TGN. This compressed organization makes it hard, if not impossible, to resolve individual TGN subdomains from other organelles by light microscopy in intact cells. Although EM-tomography provides the required resolution (Ladinsky *et al.*, 1994), it has not yet been combined with quantitative immunolocalization techniques. The second challenge is conceptual and concerns the identification of the TGN. According to the widely accepted Golgi maturation hypothesis (Glick and Luini 2011), the TGN distributes all its constituents, including proteins such as TGN38/46 or furin, which are enriched at the TGN at steady state, to different destinations and disintegrates in the process as the next-younger Golgi cisterna takes its place. Because this dissolution step involves protein segregation, it precludes the a priori assumption that any TGN protein would ubiquitously and uniformly mark both putative apical and basolateral TGN cargo subdomains.

We devised a fluorescence-based cell fractionation approach that overcomes these two limitations for an assessment of apical-basolateral cargo segregation at the TGN: 1) To achieve better spatial resolution, we convert the 3D compartmental organelle organization into a microsomal fraction that is spread out in two dimensions on a coverslip. 2) To identify the apical and basolateral cargo populations in the TGN, we accumulate fluorescently tagged cargo via a pulse-chase regimen in the 20°C compartment, identify microsomes from posterior compartments in the biosynthetic pathway (i.e., ER and *cis*/med/*trans*-Golgi) by immunofluorescence (IF) analysis of established organelle markers, and infer TGN-microsomes by exclusion. Using this novel assay, we compare the extent of protein segregation at the TGN of proteins with similar and different post-Golgi itineraries. We also determine how apical-basolateral protein sorting at the TGN compares with their segregation in post-TGN compartments along the exocytic route.

RESULTS

Our strategy to quantify protein sorting in the TGN and post-TGN compartments required the solution to three problems: 1) identifying the TGN population of a cargo pair, 2) spatially resolving the TGN from other organelles, and 3) distinguishing true cargo sorting from cargo segregation due to differences in expression levels and/or efficiency in ER-to-Golgi transport of the reporter proteins.

A pulse-chase protocol to enrich and identify the TGN population of membrane cargo in the secretory pathway

To identify cargo in the TGN, we devised a pulse-chase regimen in which we cotransduce Madin–Darby canine kidney (MDCK) cells with two recombinant adenoviruses each encoding a cargo protein. The cargoes were engineered to oligomerize in the ER, preventing them from being packaged into COPII vesicles for Golgi delivery from ER exit sites. Reversible ER aggregation of VSVG cargo was achieved by a 40°C temperature incubation using the well-characterized temperature-sensitive mutant VSVG ts045 (Kreis and Lodish, 1986). The apical model cargoes NTRp75 and green fluorescent protein (GFP)-tagged dipeptidylpeptidase IV (DPPIV) were endowed with a luminal conditional aggregation domain (CAD) based on four copies of the FKB12 moiety, which mediates constitutive aggregation that can be reversed by low concentrations of rapamycin or rapamycin derivatives (Rivera *et al.*, 2000). The fluorescent proteins (FPs) of fluorescently tagged cargo were added to the cytosolic tail, whereas a cytosolic tail antibody was used detect NTRp75-CAD over the course of experiments. After an overnight synthesis of the cargo protein pair under nonpermissive conditions, the aggregation was reversed, and the cargoes were chased from the ER through the Golgi to the TGN by adding rapamycin for CAD-containing proteins and shifting the cells to a temperature of 20°C, a temperature at which exit of most membrane cargo from the TGN is blocked, leading to its accumulation at the TGN (Matlin and Simons, 1983). Although its mechanism is not fully understood, the 20°C block has been shown not to block glycosylation of nascent proteins in the Golgi and also not to disrupt Golgi organization but only to increase the volume of the otherwise functional TGN-tubules, as seen by EM tomography (Matlin and Simons, 1983; Ladinsky *et al.*, 1999). In addition to not disrupting Golgi function, clathrin and lace-like protein-coated budding structures have been observed on TGN tubules under conditions of a 20°C accumulation, indicating that transport carrier formation and, likely, membrane protein sorting are not

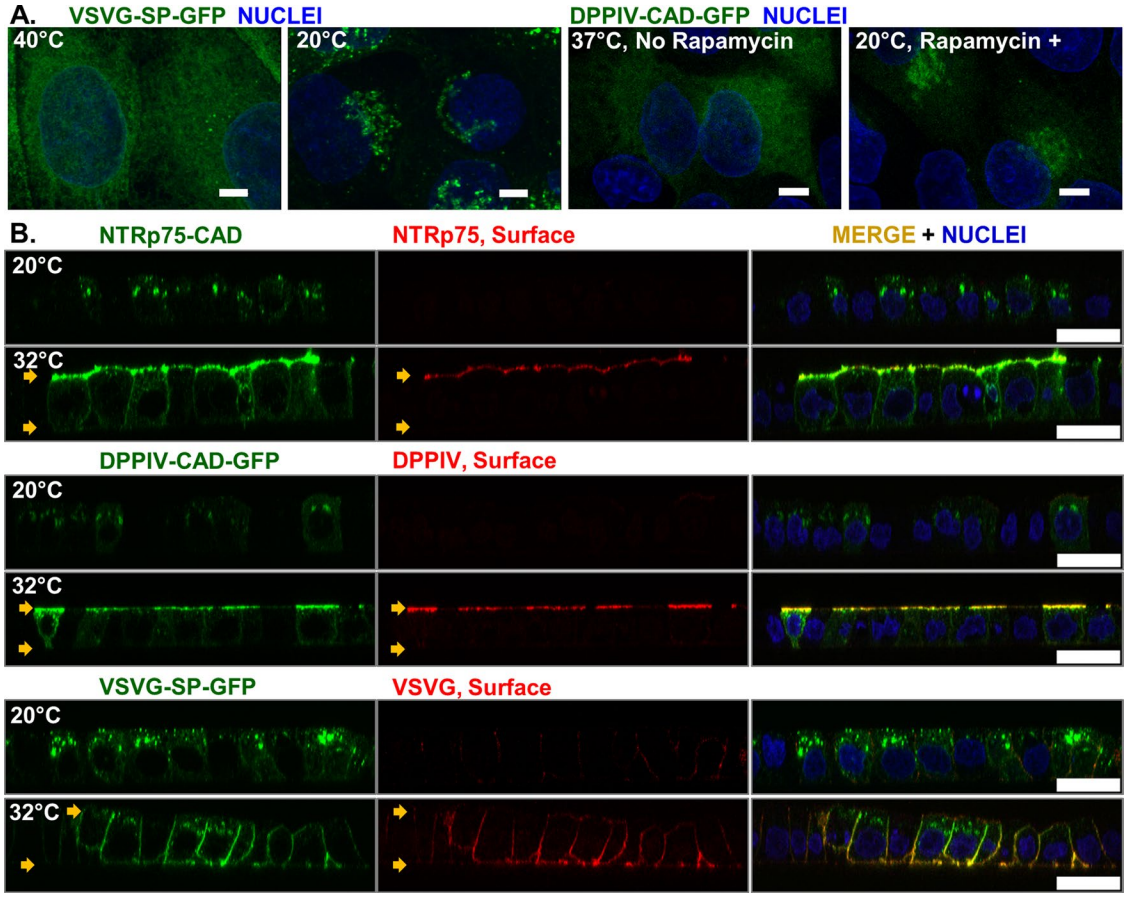

FIGURE 1: Polarized surface appearance of VSVG-SP-GFP, CAD-NTRp75, and CAD-DPPIV-GFP is controlled by a pulse-chase regimen. (A) The *xy*-projections of MDCK cells transduced with VSVG-SP-GFP or DPPIV-CAD-GFP, showing initial accumulation of cargo in the ER at 40 or 37°C in the absence of rapamycin, followed by chase to the Golgi at 20°C and after addition of 3 µM rapamycin. (B) The *xz*-projections showing surface populations of NTRp75-CAD, DPPIV-CAD-GFP, and VSVG-SP-GFP before and after surface release from 20°C block. Anti-NTRp75, anti-DPPIV, and anti-VSVG ectodomain antibodies were applied to cells before fixation (staining shown in middle panels). Arrowheads indicate top and bottom of monolayer. Left, total NTRp75 staining after fixation and total GFP signals. Scale bars, 10 µm (*xy*), 25 µm (*xz*).

interrupted at this temperature but that, instead, lack of microtubule-dependent pulling of the forming transport carriers prevents cargo from leaving (Ladinsky *et al.*, 1994). At the 20°C stage, all cargo expressed in the cell is located in the TGN, the cisternal Golgi, or the ER. Positivity for resident ER or cisternal Golgi markers would therefore be indicative of the non-TGN cargo fraction, whereas lack of ER or cisternal Golgi marker positivity would delineate true TGN cargo populations by exclusion.

We established the stages of the cargo pulse-chase ER retention and TGN accumulation at the 20°C block (Figure 1A), as well as the steady-state polarized distribution of cargo after the 20°C block release and delivery to the plasma membrane, in MDCK II cells. The absence of cargo from the cell surface during ER and TGN accumulations and the subsequent surface arrival of cargo was confirmed by staining the cells with appropriate ectodomain antibodies at 4°C after the different stages of the pulse-chase but before fixation (Figure 1B). Confocal images of the pulse-chased cells show strict retention of cargoes at the ER and TGN at the corresponding accumulation stages. The steady-state distributions of apical DPPIV-CAD-GFP and NTRp75-CAD proteins are restricted to the apical domain, whereas the VSVG-SP-GFP (Figure 1B) and VSVG-SP-SNAP (unpublished data) variants have a strict basolateral localization.

Converting 3D cellular organelle density into a low-density two-dimensional spread

One of the caveats to analyzing fluorescent material coming from densely packed and size-delimited organellar structures in intact cells is the resolution of the subdomains that make up such structures, particularly in the axial (*xz*) direction. To achieve better spatial resolution, therefore, we sought to eliminate sample thickness as a significant variable in imaging membrane-bound cargo derived from organelles, as well as to mechanically separate the cargo-containing membranes to resolve smaller structures physically rather than optically. We subjected the cells that were pulse-chased at 20°C to homogenization and further fractionation, so that the resulting material contained a suspension of membrane microsomes ranging in size from 100 nm to ~2 µm, with microsomes >500 nm usually being composed of multiple membrane fragments connected by filamentous milieu (Figure 2B). Immobilizing the micronized cargo fractions on glass with formaldehyde fixation allowed us to stain the cytosolic epitopes with antibodies against cargo, ER, and *cis*-Golgi markers, resulting in a two-dimensional (2D) map of antibody and FP fluorescence in the sample. In addition, we tested different conditions in which cargo was predominantly localized to intracellular pools versus the plasma membrane. Whereas cargo from intracellular organelles was efficiently marked by the cytosolic

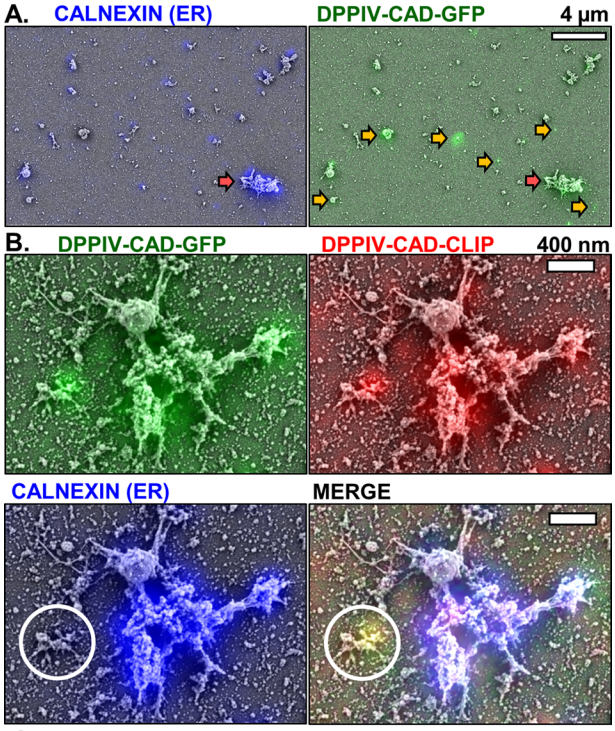

C.

	Free VSVG	VSVG + DPPIV
VSVG Alone	99.25 %	0.75%
VSVG + DPPIV, Co-homogenized	97.73%	2.27%
VSVG + DPPIV Co-Transduced	33.33%	66.67%

FIGURE 2: Sonication of cell homogenates generates discrete cargo-positive microsomes. (A) Low- (5000×) and (B) high- (20,000×) magnification correlative light–EM microscopy images of fractions from MDCK cells cotransduced with DPPIV-CAD-GFP and DPPIV-CAD-CLIP and stained with calnexin. Images in B show a field of calnexin and GFP fluorescence and the underlying membrane structures. Yellow arrows indicate GFP-positive events devoid of ER marker. Red arrows point to an aggregated structure. White circles show an aggregated calnexin-positive structure and an adjacent smaller, calnexin-negative microsome. (C) Relative number of DPPIV-CAD-GFP–positive VSVG-SP-mTagBFP events detected in fractions prepared by different homogenization methods, indicating absence of experimentally induced membrane fusion.

tail antibodies against VSVG and NTRp75, intensities detected by the respective ectodomain antibodies expressed as a fraction of the combined ectoplasmic- and cytoplasmic-domain antibody-detected intensities was used to determine the relative surface population of each cargo. Supplemental Figure S1A shows the relative surface fraction of VSVG-SP-GFP and NTRp75-CAD after the 20°C block to be 12 and 14%, respectively. During subsequent release of the 20°C block to 32°C, the respective surface fractions increased to ~20 and ~25% during the first 40 min, but after 90 min of the release, >~75% of VSVG had reached the surface, whereas that number for NTRp75 was only ~40%. We attribute this slower rate of surface arrival of NTRp75 to a more elaborate post-TGN itinerary involving a subapical distribution characteristic of the apical recycling endosome (Supplemental Figure S1B, arrowheads). Detection of intracellular cargo via the cytosolic epitope and that of surface-arrived cargo using the ectodomains additionally confirmed that microsomes formed during fractionation seal with the same orientation as their source organellar membranes.

We sought to further characterize the fidelity of our fluorescence-based imaging by comparing fluorescence and EM-based images via correlative light and electron microscopy (Figure 2, A and B). Indeed, we observed individual puncta by fluorescence that could be traced to discrete membrane structures. Larger objects and aggregates composed of multiple membrane pieces produced larger, uneven fluorescence patterns (Figure 2B; red arrows in Figure 2A) and nearly always costained for the ER marker calnexin. We were able to resolve small, discrete, cargo-containing structures that corresponded to single fluorescent puncta and were found to have no ER association despite close proximity to structures that were ER positive (Figure 2B, circled structure that contains two DPPIV cargoes and is negative for calnexin). These findings further supported the basis for our approach to identifying 20°C-derived biosynthetic TGN cargo by the absence of markers retrograde of the TGN.

Because colocalization formed the basis for our analysis of the relationship between membrane-bound proteins, it was important to test the fractionation technique for artifactual colocalization produced as a result of homogenization and sonication of cargo-containing membrane pools. We tested for potential fusion of unrelated membrane fractions and the resulting false positives in membrane fractions from cells transduced independently with either VSVG-SP-mTagBFP or DPPIV-CAD-GFP by imaging the single and colocalized events in samples that were unmixed, mixed together on the coverslip, or cosonicated before fixation. The results (Figure 2C) show virtually no contamination of the VSVG-positive fraction by DPPIV, indicating that neither mixing nor cosonication results in vesicle fusion and subsequent false colocalization.

Identification of the TGN cargo population in the microsome fraction

Using in vivo–validated antibodies against calnexin, an ER membrane protein, we determined that ~25% of VSVG-SP-GFP/mTagBFP and ~30% of CAD-containing NTRp75-CAD or DPPIV-CAD-GFP remain associated with the calnexin-positive membrane pool at the end of the 20°C block in dual-color vesicles (Figure 3A for VSVG and NTRp75-CAD; unpublished data for DPPIV-CAD-GFP) despite the predominant Golgi localization described in Figure 1A. To account for the intensities, we used a custom imaging regimen that is discussed in the next section in more detail. Releasing the 20°C block to a permissive temperature of 37°C did not decrease the calnexin-positive fraction and neither did prolonging the 2-h 20°C incubation, which furthermore proved detrimental to the fidelity of the block. This indicates that some ER aggregation of conditionally aggregatable proteins may in fact be irreversible. At the same time, <15% of the cargo microsomes proved positive for the *cis*-Golgi marker giantin (unpublished data), in spite of the good colocalization between 20°C accumulated cargo and giantin observed in cells when imaged by confocal microscopy with a 63× objective (Figure 4A). These findings indicate that our fractionation physically separated the Golgi stack from the TGN and that the cargoes accumulating in the 20°C compartment are largely cleared from the *cis*-Golgi. To ascertain that the small *cis*-Golgi–positive cargo populations do not skew the colocalization analysis of VSVG-SP-GFP and NTPp75-CAD in the 20°C compartment, we used our software to compare the correlation between the two cargo populations after immunostaining of either calnexin alone or a combination of calnexin and giantin. As shown in Supplemental Figure S2, excluding the giantin-positive fraction in

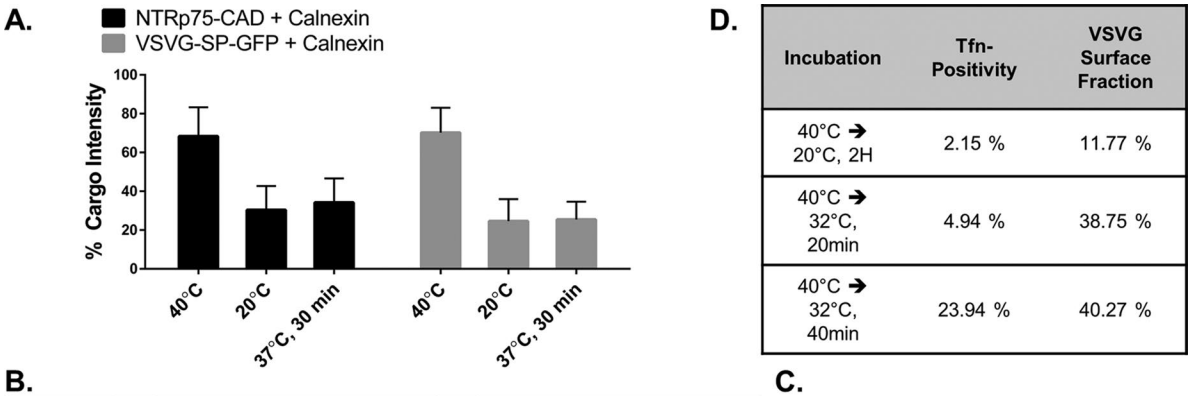

D.

Incubation	Tfn-Positivity	VSVG Surface Fraction
40°C → 20°C, 2H	2.15 %	11.77 %
40°C → 32°C, 20min	4.94 %	38.75 %
40°C → 32°C, 40min	23.94 %	40.27 %

B.

Pair	VSVG-VSVG		NTRp75-VSVG	
Species	VSVG-SP-mTagBFP	VSVG-SP-GFP	NTRp75-CAD	VSVG-SP-GFP
40°C	4.26 %	8.23 %	2.43 %	2.80 %
20°C	21.62 %	18.53 %	23.47 %	26.22 %
37°C, 30min	5.27 %	6.25 %	16.19 %	15.06 %

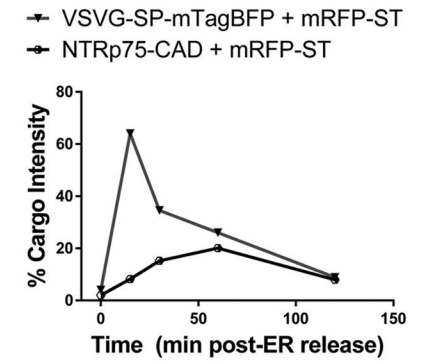

FIGURE 3: Exocytic itineraries of isolated VSVG-SP-GFP/mTagBFP and NTRp75-CAD fractions can be described by compartmental markers for ER, the Golgi apparatus, and Tfn-positive endosomes. (A) Relative fluorescence intensities of NTRp75-CAD and VSVG-SP-GFP isolated dual-color populations that stained positive for ER marker calnexin at 40 and 20°C and after a post-20°C chase at 37°C for 30 min. Fractions were collected from cells cotransduced with both cargoes. Data are from four experiments. (B) Relative sialyltransferase enrichment of VSVG-SP-GFP/mTagBFP and NTRp75-CAD dual-color populations for the same pulse-chase time points as in A. Fractions were isolated from cells expressing mRFP-ST after cotransduction with either two basolateral or an apical and basolateral cargo pair. (C) VSVG-SP-mTagBFP and NTRp75-CAD enrichment of the mRFP-ST compartment during a post-ER chase at 32°C. (D) hTfn-594/568-positive fraction of VSVG-SP-GFP/mTagBFP and the corresponding relative surface fraction measured by ectodomain and cytosolic tail antibody staining during the 20°C block or 20 and 40 min of post-ER chase at 32°C.

addition to the calnexin-positive population did not change the apparent cargo correlation.

On the basis of these results, we conclude that due to its retention of aggregated cargo, the ER is the main source of non-TGN cargo at the end of the 20°C block, and we thus describe the TGN population as the calnexin-negative fraction in our analysis.

Using a cell line expressing monomeric red fluorescent protein (mRFP) linked to the targeting motif of sialyltransferase (mRFP-ST; Salvarezza *et al.*, 2009), we tested cotransduced basolateral–basolateral and apical–basolateral cargo pairs for relative enrichment of the sialyltransferase compartment. We found that the intensity fraction of VSVG-SP-GFP/mTagBFP and of NTRp75-CAD that colocalized with mRFP-ST increased, respectively, from ~5 and 2% at 40°C to ~20 and 23% in the 20°C compartment in both pairs (Figure 3B). When cargo was allowed to exit the TGN for 30 min after the release of the 20°C block, the mRFP-ST–positive fraction dropped to ~6% for VSVG-SP-GFP/mTagBFP in a basolateral–basolateral pair but was higher for both VSVG-SP-GFP and NTRp75-CAD in the apical–apical pair, reaching 15 and 16%, respectively (Figure 3B), suggesting that individual cargo pairs differ in their kinetics through the exocytic pathway. The low degree of colocalization between mRFP-ST and nascent cargo during the 20°C block was somewhat surprising, given that sialyltransferase has been localized to both the *trans*-Golgi cisterna and the TGN (Roth *et al.*, 1985; Rabouille *et al.*, 1995). Our observation is not due to an underrepresentation of mRFP-positive microsomes in the sample compared with VSVG-SP-GFP vesicles, as only <15% of total mRFP-ST intensity detected in the samples was observed to colocalize with cargo (unpublished data). Moreover, we transiently detected a much higher degree of colocalization between both proteins when we followed the VSVG-SP-GFP population exiting the ER at 32°C. A peak of ~65% mRFP-ST-positive VSVG was apparent within the first 15 min of the chase (Figure 3C). Although the enrichment of mRFP-ST with apical NTRp75-CAD was slower and produced a broader peak that reached a maximum of ~20% after 1 h of the post-ER chase, after 60 min, the mRFP-ST compartment was de-enriched from both cargoes. Taken together, our findings in Figure 3, A–C, suggest that the anterograde cargo-containing domains of the TGN are largely distinct from the *trans*-Golgi and TGN domains enriched in resident Golgi enzymes.

Finally, we analyzed the colocalization of cargoes with transferrin (Tfn)-positive endosomes. We established the absence of cargo from the Tfn-positive compartment at 20°C by analyzing homogenized fractions of filter-grown MDCK cells expressing human transferrin receptor (hTfR) equilibrated with hTfn–Alexa 594 or –Alexa 568 that was offered in the apical and basolateral chambers (Supplemental Figure S3). We found that only ~5 and ~2% of DPPIV and VSVG

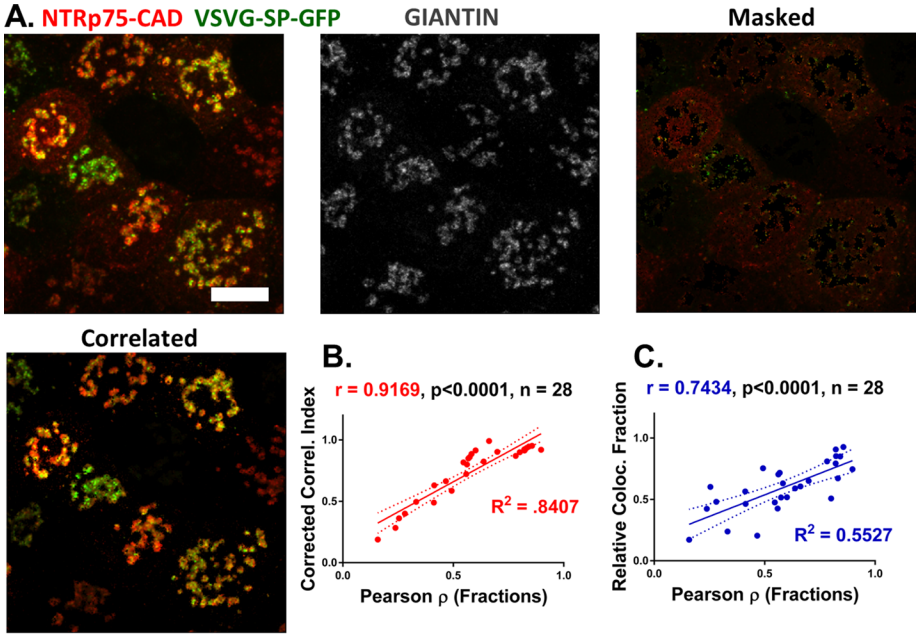

$$\text{Corrected Correlation Index (CCI)} = \frac{\text{Pearson } \rho \text{ (Fractions)}}{\text{Pearson } \rho \text{ (Cells)}}$$

FIGURE 4: The description of true cargo colocalization requires correction for intercellular variation. (A) Sample of unfractionated cells cotransduced with NTRp75-CAD and VSVG-SP-GFP kept for confocal analysis, showing intercellular variability in expression. Cells are costained with giantin, which fully overlaps with the 20°C-blocked cargo. Region-of-interest masks of Golgi regions are made, and correlation between cargo channels within the masks is measured. The correlation measured in cells serves as a theoretical maximum and is used to normalize the correlation measured in isolated cargo fractions, yielding a corrected correlation index. (B) Correlation between raw Pearson values measured in vitro and the corrected correlation index values obtained from the same experiments. (C) Correlation between raw Pearson values and the relative colocalized fractions of cargo from same experiments. Thr Manders coefficients obtained for cargoes in Golgi ROIs are used to correct the values of relative colocalized fractions.

events, respectively, were positive for Tfn-594 (Figure 3D), indicating the robustness of the 20°C block in keeping exocytic cargo from the recycling compartment. On the other hand, after release of the ER-accumulated VSVG-SP-GFP population at 32°C, the Tfn-positive fraction of VSVG-SP-GFP increased from ~5% after a 20-min chase to ~25% at the 40-min chase time point (Figure 3D). This is in agreement with the reported passage of VSVG through Tfn-accessible endosomes during its TGN-to-surface itinerary (Ang *et al.*, 2004; Cresawn *et al.*, 2007; Gravotta *et al.*, 2012). The absence of a corresponding increase in VSVG ectodomain antibody staining during the 20- to 40-min transition (Supplemental Figure S1) indicates that the evolution of VSVG-Tfn positivity occurred while the cargo was en route to the cell surface.

Taking our results together, we conclude that our marker analysis faithfully reflects the itineraries of exocytic cargoes.

An algorithm to quantify true cargo sorting at the TGN

To obtain quantitative information on cargo distribution from the calnexin-negative fractions of homogenized membrane samples, we optimized image acquisition and analysis procedures. Imaging was done using a 100× wide-field, color-corrected numerical aperture (NA) 1.4 lens coupled to a charge-coupled device (CCD) camera. For accurate representation of cargo intensities, exposures for different cargo fluorescence were maximally stretched over the 12-bit dynamic range of the CCD, and cargo fluorescence was detected in the visible light spectrum (see *Materials and Methods* for the tags and antibody fluorophores used for cargo detection). The far-red region, which the CCD detects with less efficiency, was reserved for calnexin, since ER positivity was confirmed based on marker presence alone rather than the extent of marker–cargo correlation. To control for instrument noise and staining specificity, for each experiment, we duplicated the immunofluorescence and imaging protocol using fractions collected from untransduced MDCK cells and prepared in the same way as the cargo-containing samples. In none of the analyses did the control staining account for >10% of specific intensity detected in the cargo channels from transduced samples.

Micronized membrane fractions confer low signal-to-noise ratio and are devoid of structural information. We developed a custom algorithm to discriminate for peaks produced by fluorescence clusters on membrane particles from signal produced by instrument noise, unspecific fluorescence, dirt, and aggregated fluorescent structures. The program reports peak overlaps (within specified error based on centroid shifts) between images, together with their peak volumes (integrated intensities). The peaks are identified by shape. Supplemental Figure S4 schematically illustrates for the peak selection criteria. A peak is called if its intensities in the *x*- and *y*-directions fit a Gaussian envelope. Both minimum and maximum circumference and intensity of a peak can be controlled directly through a set of options. Supplemental Figure S5 shows two examples of peaks that either passed or failed the Gaussian criteria, demonstrating how the fitting can identify a peak in samples that are either aggregated or have a questionable pixel distribution.

Data obtained from the chosen peaks were used to describe the degree of colocalization and segregation by two parameters: on the basis of the assumption that for two cargoes to be truly cosorted, they have to maintain a linearity in their relationship, we determine the Pearson coefficient for the intensities of two cargoes in objects where both cargoes are colocalized. For correlation analysis, therefore, we used dual-cargo-containing fractions after subtracting the calnexin-positive dual-cargo pool (characterized in Figure 3A). We also determine the intensity of single, noncolocalized objects and find the relative ratio of combined intensities of all single and colocalized objects for each cargo. Because one cargo is usually more abundant in any given sample due to differences in protein levels and detection efficiency, it therefore registers noncolocalized events that are due to overabundance rather than genuine sorting. We therefore always report the colocalization fraction for the least abundant cargo in the pair. When plotting the Pearson coefficient against the corresponding relative colocalization fraction from each of the 28 samples analyzed for this study, we observed an interdependently increasing relationship between the two terms with a Pearson coefficient of 0.74, indicating that the two values are

indeed correlated (Figure 4C). Thus a low correlation of cargo in dual-cargo objects is associated with more microsomes that contain only single cargoes.

Because our vesicles are pooled from many cells, any cell-to-cell variation in the intensity profiles of each cargo in the Golgi due to differential expression or transport rates from the ER to the Golgi results in a reduced maximum correlation that we can observe upon fractionation analysis and artificially increases the relative number of single cargo positives independently of true cargo segregation. To account for this, we devised a simple strategy to correct the measurements obtained from our in vitro analysis by the data that we could obtain regarding cargo variability from cells before fractionation. We placed two coverslips into the culture dish before plating monolayers to be collected for fractionation. The coverslips were recovered and fixed immediately before fractionation. We used a giantin labeling or the signal of the mRFP-ST to delineate the Golgi and the TGN and took confocal stacks of multiple fields of view in cells with a 63× objective. At this level of resolution, giantin and sialyltransferase localization appear indistinguishable from the TGN and mark the cargo-positive TGN enriched compartment well (Figure 4A). We then used the two markers to make masks of the Golgi area and obtained a Pearson and a Manders coefficient for the two cargo protein intensities within the masks. Because we measured over a field of view of many cells, the coefficients we obtained reflected true cell-to-cell variability. Furthermore, since we could not resolve individual domains in the TGN at this level of resolution, the Pearson value obtained reflected a theoretical maximum correlation between two cargoes due to non–sorting-related factors. We therefore normalized our in vitro measured Pearson values to obtain a corrected correlation index (CCI). The Manders coefficient, reported for each cargo, reflects the percentage of that cargo in colocalization with the other. The only source of noncolocalized cargo intensities within Golgi masks we produced were cells that were not transduced with both cargoes. The Manders coefficient measured in the Golgi masks therefore produced a theoretical maximum for the relative colocalized cargo fraction that we measure in vitro. Accordingly, we normalized the relative colocalization values from the in vitro data by the Manders coefficients measured.

In Figure 4B, we compare the CCI to raw Pearson values obtained in vitro in the same manner as we did before to test the linearity between the two types of summary statistics. We observed a Pearson coefficient of 0.92, which indicates a very linear relationship.

Apical–basolateral cargo pairs are more segregated at the TGN than are apical–apical and basolateral–basolateral pairs

Figure 5 summarizes the workflow we followed to characterize the sorting profiles of three membrane-bound cargo pairs at the TGN; we paired proteins based on their likelihood of affinity at various stages of the secretory pathway. VSVG-SP-GFP paired with VSVG-SP-SNAP or VSVG-SP-mTagBFP served as the highest theoretically correlated example due to the trimeric nature of VSVG protein under normal conditions (i.e., even when conditionally deaggregated). The different trimers of VSVG would be expected to randomly incorporate either of the two differently tagged copies of the protein produced as a result of cotransduction, and these trimers would be expected to stay constant throughout the endomembrane sorting events and subsequent plasma membrane delivery. The double-VSVG pair therefore served as a positive control for observing the highest correlation and colocalized event distribution values possible using our methodology. Using our assay and analysis strategy after 20°C accumulation to this cargo pair, we obtained a Pearson value of 0.85, which is high for a biological sample (Table 1). The CCI and relative colocalization values for the VSVG-VSVG pair were 0.92 and 79.68%, respectively, indicating a high correlation of the two complexed proteins by all three parameters.

In comparison, the pairing of two apical proteins, NTRp75-CAD and DPPIV-CAD-GFP, was used to represent a scenario for two proteins with the same destination but without any physical complexing, as in the case of two VSVG-ts045 proteins (Table 1) There is evidence that apical proteins, which depend on the incorporation into lipid rafts for apical sorting, follow a different post-Golgi itinerary than apical proteins, which are clustered by raft-independent mechanisms (reviewed in Weisz and Rodriguez-Boulan, 2009). Because apical targeting of NTRp75-CAD and DPPIV-CAD-GFP occurs lipid-raft independently, we predicted that the pair would travel together. The raw Pearson coefficient (0.65) and colocalized fraction (62.87%) were decreased in this sample relative to the VSVG-VSVG pair, but much of this is attributable to the differences in expression in the 20°C compartment, as indicated by the improvement in the CCI measurement of 0.93.

The last pairing was of basolateral VSVG-SP-GFP and apical NTRp75-CAD. This pair was used to represent a scenario of heterotypic proteins with diverging destinations and targeting routes. The raw Pearson coefficient of 0.54 and the CCI of 0.74 indicate a clear difference between sorting of this apical–basolateral pair and the complexed and homotypic cargo pairs at 20°C and support the notion of sorting of VSVG-SP-GFP and NTRp75-CAD at the TGN. The colocalized fraction of 72.47%, on the other hand, was as strong as for the other two pairs, given the SD of the samples (Table 1). This implies that whereas TGN-accumulated cargo was largely separable from cisternal Golgi and TGN-resident Golgi proteins at 20°C (Figure 3), segregation of apical and basolateral cargo into physically separable entities had not occurred to the same extent. Taken together, the decrease in Pearson and CCI values supports the long-held view of the TGN as a sorting station, yet the relatively high number of colocalized events suggests that the sorting might not be complete at 20°C.

Apical and basolateral cargo sorting is not complete in the TGN but continues in post-TGN compartments

To resolve whether protein segregation at the TGN alone accounts for the highly polarized surface delivery of apical and basolateral cargoes, we determined what happens to the sorting profiles of cargo after it leaves the TGN. To this end, we extended our analysis of the cargo pairs to three additional time points after releasing the 20°C temperature block to 32°C. At 20 min, the colocalization of each of the cargoes with giantin determined from 63× confocal images of fixed cells decreased substantially across the three pairs (Figure 6B), but little (VSVG-SP-GFP/VSVG-SP-SNAP) or no (VSVG/NTRp75-CAD and NTRp75-CAD/DPPIV-CAD-GFP) surface arrival was evident (Figure 6A, arrows). We consider this a time point at which most of the cargo is in transit to the cell surface. At 40 min, surface arrival became more apparent, concomitant with further decrease in cargo colocalization with giantin for all pairs, and NTRp75-CAD and DPPIV-CAD-GFP began to be enriched in a subapical endosome (Figure 6A, arrowheads). Consistent with limited detection of ectodomain epitopes on cargo fractions isolated at 20 and 40 min after 20°C release, as shown in Supplemental Figure S1, these two time points represent the transit of post-Golgi cargo before complete surface arrival. At 90 min, surface arrival was likely complete (Figure 1), and postendocytic events are expected to contribute significantly to the intracellular cargo distribution. On exit from the

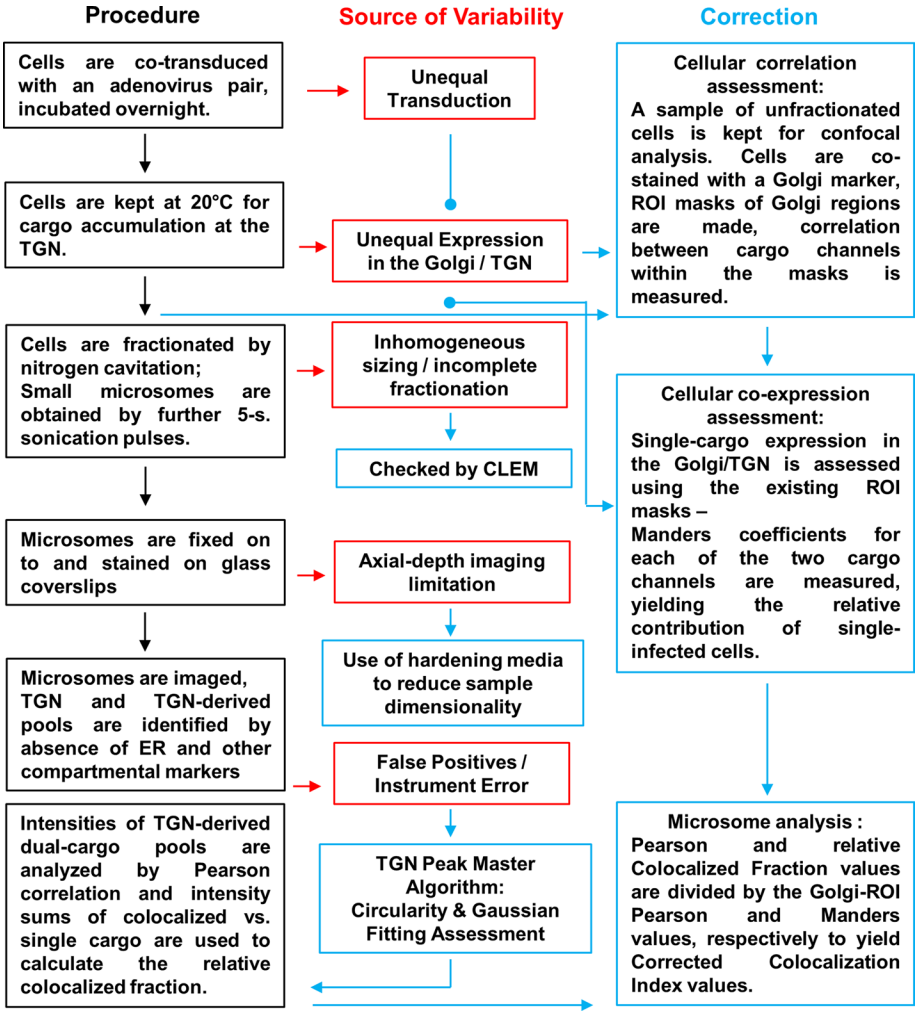

FIGURE 5: Analysis workflow.

TGN, a progressive increase in the percentage of single-cargo vesicles and a corresponding decrease in the fractions of vesicles that contain both cargoes occur during the post-TGN chase regardless of additional post-TGN sorting because apical and basolateral proteins are ultimately separated for delivery to distinct surface domains. Therefore only the evolution of the Pearson coefficient and the CCI and not of the single-to-colocalized cargo ratio is a meaningful parameter to gauge additional sorting steps. The changes in raw Pearson and CCI values from the 20°C data (Table 1) along this time course are shown in Figure 7. The complexed VSVG-SP-GFP and VSVG-SP-SNAP proteins, as expected, remain most tightly associated at all time points. The apical pair NTRp75-CAD and DPPIV-CAD also maintained a high correlation index. By contrast, not only did the NTRp75-CAD/VSVG-SP-GFP pair have a lower correlation in the 20°C compartment than did the other two pairs, but the Pearson and CCI values further decreased at each post-TGN chase point. To investigate whether the Pearson correlation is indeed the appropriate statistic to describe the differences between time points within the same and between different protein pairs during the time course, we performed bootstrap statistical analysis of the data from the calnexin-negative colocalized distributions of the cargo pairs taken at each time point. We then constructed confidence intervals for the Pearson summary statistic (Supplemental Figure S6). We draw the following conclusions from this analysis: 1) The mean and interval values for VSVG-SP-GFP/VSVG-SP-SNAP and NTRp75-CAD/DPPIV-CAD-GFP do not change from one time point to the next with any significance (the large confidence interval for the 20-min time point for NTRp75-DPPIV is due to its being derived from only a single experiment), supporting the notion that their association changes little throughout their TGN and post-TGN itineraries. 2) The confidence interval of the NTRp75-CAD/VSVG-SP-GFP pair is larger at 20°C and then further widens during the 20- to 40-min post-TGN progression, indicating that colocalized cargo intensities of these two proteins become more variable after the cargo pair leaves the TGN. Differences between the means of the confidence intervals reflect the differences in raw Pearson correlation curves in Figure 7A, which have not been corrected for intercellular variability but indicate that raw Pearson coefficient means of each pair are significantly different. Taken together with the CCI measurements (Figure 7B), the analysis of the confidence intervals is consistent with ongoing apical–basolateral protein sorting after cargoes leave the TGN.

DISCUSSION

We devised a pulse-chase regimen and a coupled cell fractionation and fluorescence imaging protocol that allowed us for the first time to describe quantitatively the sorting process of apical and basolateral proteins in the Golgi and post-Golgi legs of the exocytic pathway. When corrected for cell-to-cell intensity differences of two cargo proteins in the total Golgi population, the Pearson coefficient

Pair	VSVG-ts045-GFP/ VSVG-ts045-SNAP	NTRp75-CAD/ DPPIV-CAD-GFP	NTRp75CAD/ VSVG-ts045-GFP
Type	BL:BL (trimerizing)	AP:AP	AP : BL
Pearson correlation	0.8471 ± 0.0435	0.6480 ± 0.0597	0.5410 ± 0.0421
Corrected correlation index	0.9186 ± 0.0040	0.9265 ± 0.0563	0.7445 ± 0.1398
Colocalized fraction (%)	79.68 ± 5.33	62.87 ± 2.26	72.47 ± 2.58

Data are from three experiments. AP, apical; BL, basolateral.

TABLE 1: Cargo correlation at the end of the 20°C block is lowest for the apical–basolateral cargo pair.

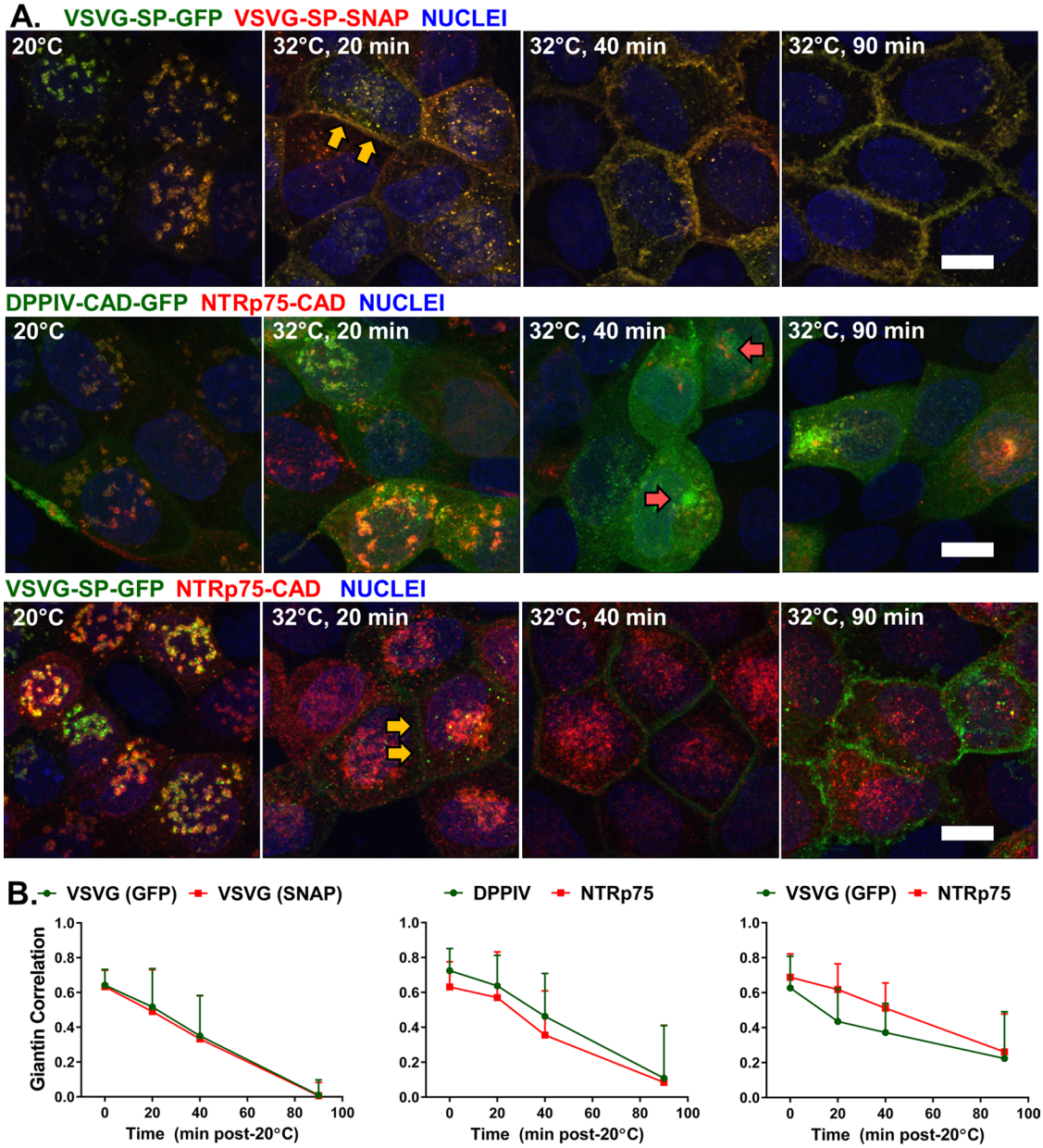

FIGURE 6: Cargoes synchronously exit the Golgi after temperature switch from 20 to 32°C. (A) The *xy*-projections of cells cotransduced with VSVG-SP-GFP/VSVG-SP-SNAP (top), DPPIV-CAD-GFP/NTRp75-CAD (middle), or NTRp75-CAD/VSVG-SP-GFP (bottom) during and after the release of the 20°C block and the chase to the cell surface. Yellow arrows at 20 min indicate basolateral surface arrival of VSVG-SP-GFP. Red arrows at 40 min indicate subapical endosomal localization of DPPIV-CAD-GFP and NTRp75-GFP, which is also seen at 90 min. (B) Correlations of the chased pairs with *cis*-Golgi marker giantin, as measured by line-plot profiles drawn across the Golgi region in the cells, used as indicators of Golgi exit dynamics for each cargo in the pair.

describing the correlation of two cargo intensities within the cargo-containing microsomes yielded a sensitive quantitative description of protein segregation at different steps of the secretory pathway. A high Pearson correlation was always associated with a large colocalized cargo fraction, that is, a large fraction of the total intensity of the less abundant cargo was also positive for the more abundant protein of the pair. We never observed a high Pearson coefficient accompanied by a small colocalized cargo fraction. This rules out bipartite scenarios in which one population of a cargo pair is perfectly colocalized, whereas the other population is entirely separated. Instead, the correlation between the two values suggests that single-cargo events can be treated as an extreme of poor cargo intensity correlation in dual-cargo vesicles. On the other hand, we were able to resolve sorting differences between cargo pairs that had comparable colocalized fractions based on their different Pearson coefficients (Table 1). Furthermore, given the nature of our data sets as bivariate intensity distributions, it was possible to perform a bootstrap analysis to calculate the confidence intervals of our statistic in order to assess its significance. The calculated intervals for the two basolateral–basolateral and apical–apical pairs show little change from the 20°C to the post-TGN stages, but confidence intervals of apical–basolateral pairs become very large during the

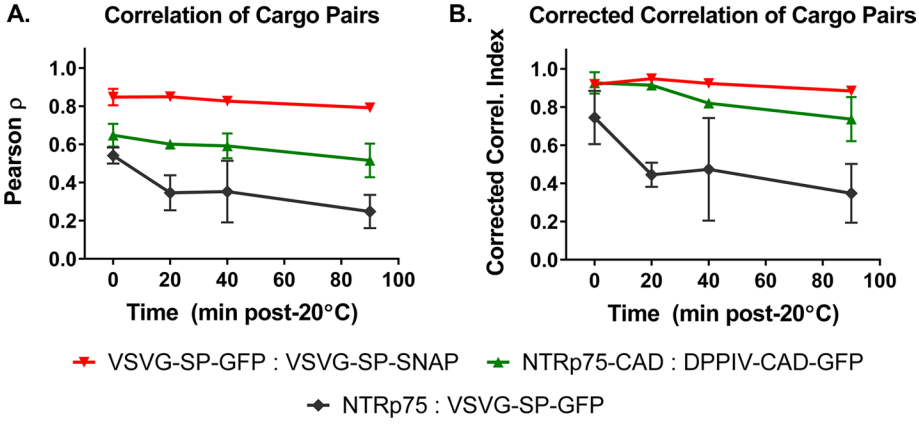

FIGURE 7: Correlation of the apical–basolateral cargo pair further decreases after the release of the 20°C block. Pearson correlations (A) and CCI values (B) for three cargo pairs at the end of the 20°C block and 20, 40, and 90 min after the switch to 32°C. The 20°C and 90-min post-TGN time points were constructed using means from three experiments, except for VSVG-VSVG 90-min post-20°C, which was obtained from two experiments. The 20- and 40-min time points were constructed using means from two experiments, except for the NTRp75-DPPIV 20-min point, which was measured in a single experiment.

post-TGN time course, suggesting that the decrease of Pearson values is coupled to higher variability between cargo intensities and reinforcing the notion inferred from Pearson coefficients that NTRp75 and VSVG are progressively less linearly correlated during the post-TGN chase.

Critical to our approach was the identification of the cargo population in the TGN independently of a TGN marker, which is in contrast to previous cell-based colocalization assays. We realized this after detecting that only a small fraction of VSVG-SP-mTagBFP or CAD-DPPIV-GFP colocalized with the *trans*-Golgi and TGN marker mRFP-ST in the microsome fraction when the cargoes accumulated in the 20°C compartment or after release of the 20°C block. The poor colocalization between the cargoes and the Golgi-resident marker is not due to detection limits, because we observed high transient colocalization between VSVG and mRFP-ST after a synchronous wave of the cargo left the ER. Furthermore, cargo and mRFP-ST colocalize well after the 20°C block at the resolution level of confocal microscopy in intact cells, suggesting that the recombinant marker faithfully localizes to the Golgi apparatus. We suggest that our assay resolves the segregation of cargo from resident proteins of the Golgi apparatus, which has been proposed previously (Patterson *et al.*, 2008). Such segregation at the TGN is indeed predicted by the Golgi maturation hypothesis, according to which sialyltransferase is retrieved to the proximal Golgi cisterna via COPI-mediated vesicle transport, whereas cargo is recruited into anterograde carriers. Our data indicate that VSVG and NTRp75 are segregated to a larger extent from sialyltransferase at the TGN than they are from each other.

Our most important new insight concerns the role of the TGN as central sorting station for apical and basolateral proteins. Although cargo pairs comprising two apical proteins exhibited higher Pearson correlation than the apical–basolateral cargo pair in the 20°C compartment, these differences became far larger after the proteins exited the TGN toward the cell surface, 20 and 40 min after the release of the 20°C block. We cannot rule out that the temperature switch from 20 to 32°C per se caused additional protein segregation at the TGN. For two main reasons, however, we consider it unlikely that this accounts for the observed evolution of the Pearson coefficient: 1) VSVG has been shown by immuno-EM to become enriched in discrete TGN domains during the 20°C block present as nascent buds with a cytoplasmic coat (Griffiths *et al.*, 1985). Similarly, EM tomography of the Golgi apparatus revealed the accumulation of budding structures with distinct coats on different TGN tubules at 20°C (Ladinsky *et al.*, 2002). These observations suggest that cargo sorting is effective at 20°C. 2) The increase in segregation that we measured occurred in a continuous manner and in parallel with a decrease in cargo colocalization with the Golgi marker giantin rather than in a switch-like manner and before loss of Golgi localization. Therefore we propose a model in which the TGN is not the sole sorting station for proteins in their exocytic pathway but post-Golgi compartments play a critical role in an iterative sorting process.

At least two, not mutually exclusive, mechanisms could be envisioned for post-Golgi sorting. The CRE, which mediates sorting of apical and basolateral proteins in the recycling pathway (Wang *et al.*, 2000; Thompson *et al.*, 2007) and in plants doubles as the most *trans* Golgi cisterna (Reyes *et al.*, 2011), is the best candidate to operate as an additional sorting station in the exocytic pathway. As for the TGN, resolution and identification of the CRE is challenging. It closely abuts the TGN in the perinuclear region and lacks a unique identifying marker. Both features likely contribute to the controversy regarding exocytic cargo trafficking through the CRE. We anticipate that our pulse-chase regimen for cargo pairs combined with our ability to physically separate TGN and CRE will allow us to resolve whether apical and basolateral cargoes colocalize in Tfn-positive vesicles after the release of the 20°C block, using the assay described here. It is likely, however, that not all proteins traverse recycling endosomes in their biosynthetic route (reviewed in Weisz and Rodriguez-Boulan, 2009). Whether these are more effectively sorted from other exocytic cargo in the TGN or undergo further post-TGN sorting in nonendosomal compartments also remains to be determined in future work. Apart from the CRE, the tubular transport carriers that have been observed leaving the Golgi by live-cell imaging in polarized epithelial cells and in nonpolarized cells could be sites for post-TGN sorting. Indeed, two apical proteins, sucrase-isomaltase and actase-phlorizin hydrolase, which are sorted by lipid raft–dependent and –independent mechanisms, respectively, have been observed separating from each other after they exit the Golgi in common tubular structures and as they move toward the cell surface (Jacob and Naim, 2001), although their segregation was subsequently pinpointed to a postendosomal step in the exocytic route (Cramm-Behrens *et al.*, 2008). The two apical proteins studied here both undergo raft-independent sorting. However, it was not known whether they followed a similar post-Golgi itinerary. A common route for DPPIV and NTRp75 is indeed supported by our analysis: not only did we observe both proteins traverse a prominent common subapical endosomal compartment before their arrival to the apical surface, but, of importance, our in vitro assay determined that both remained colocalized to the same extent throughout their TGN-to-surface passage. By analyzing the colocalization of cargo pairs in reference to that of a gold standard, VSVG-VSVG, we will be able in the future to compare sorting of the same cargo pairs between

different epithelial cell types that target apical proteins either directly or via transcytosis from the basolateral surface to the apical domain in order to determine whether and where they differ in their apical–basolateral protein sorting (Treyer and Musch, 2013). Our novel approach also has the potential to test hypotheses regarding sorting mechanisms that have been difficult to address in intact cells, such as where galectins, which might enter the endomembrane system via endocytosis from the plasma membrane, meet apical cargoes to promote their clustering (Delacour *et al.*, 2009) or the precise sites of action for different clathrin adaptors during the basolateral trafficking itinerary (Gravotta *et al.*, 2012; Guo *et al.*, 2013).

In sum, our study contributes to the emerging view that all intracellular sorting is an iterative process rather than a series of crossroad decisions, and our novel approach is poised to complement cell-based approaches to elucidate more of its details.

MATERIALS AND METHODS

Cell lines, transferrin uptake, and adenoviruses

We performed experiments in untransfected MDCK II cells, except for experiments in Figure 3, for which we used mRFP-ST–expressing (Salvarezza *et al.*, 2009) MDCK-Par1b Tet-OFF cells kept in the presence of doxycycline, and the transferrin–Alexa 594/Alexa 568 colocalization analysis, for which we used hTfR-expressing MDCK clones. Both lines were generated for this study. For experiments described in Figure 1 and Supplemental Figure S1, cells were cultured on polycarbonate filters; for all other cargo transduction of polarized monolayers and subsequent fractionation or imaging experiments, cells were plated at densities of 100,000 cells/cm^2 (200,000 for Tet-OFF clones) on 15-cm dishes and allowed to reach confluence for 1 d and then further polarized for 24–48 h. Adenoviruses were amplified and stored according to Falck-Pedersen (1998), and their concentration was normalized to the volume of medium used for the infection. Cargo-encoding adenovirus or a pair of cargo-encoding adenoviruses were applied to cells in S-MEM (Thermo Fisher Scientific, Waltham, MA) at concentrations optimized for single expression or coexpression, not exceeding 2% ratio of storage buffer to S-MEM. For the analysis of Tfn-VSVG colocalization in the 20°C compartment (Figure 3D and Supplemental Figure S1, 50 µg/ml hTfn–Alexa 594 or –Alexa 568 (Thermo Fisher Scientific) conjugate was added in Opti-MEM during the last 40 min of the 20°C cargo chase to the TGN from both filter chambers. To assess the endosomal itinerary of VSVG in the biosynthetic pathway (Figure 3D), we took into account that Tfn cycling is largely limited to early endosomes at 20°C and requires higher temperature for equilibration throughout the entire endosomal compartment, including the common recycling endosome (Ren *et al.*, 1998; Wilcke *et al.*, 2000). We performed the equilibration at 40°C during the ER incubation stage of VSVG-SP-GFP and collected cargo fractions at either 20 or 40 min after ER release at 32°C.

cDNAs

The VSVG-SP-mTagBFP and VSVG-SP-SNAP cDNAs were generated by replacing the GFP moiety of the VSVG-SP-GFP construct (Toomre *et al.*, 1999; provided by K. Simons, Max Planck Institute for Developmental Biology, Dresden, Germany). The source for the CAD-domain was the *Eco*RI–*Spe*I fragment of the $_{P}C_4S_1$-F_M4-FCS-hGH vector from the ARGENT Regulated Secretion Aggregation Kit (Ariad Pharmaceuticals, Cambridge, MA). The hNTRp75 sequence was appended 3′ to the F_M4 domain via the linker 5′-GAAGCTG-CAGCGAAAGAGGCTGCGGCAAAG-3′. Rat liver DPPIV (Weisz *et al.*, 1992; cDNA provided by O. Weisz, University of Pittsburgh Medical School, Pittsburgh, PA) was cloned via *Bam*HI–*Hin*dIII sites into the pEGFP-C3 vector and the GFP-fusion construct appended to the F_M4 moiety via the spacer 5′- GATCCAATTGCAATGATCAT-CATGACAGATCTGCGCGCGATCGATATCAGCGCTTTAAATTTGC-GCATGCTAGCTATAGTTC-3′. Adenoviruses were generated with the pCMV shuttle vector according to He *et al.* (1998).

Cargo pulse chase

For ER accumulation, single or cotransduced cells were incubated for 12 h at either 40°C (when VSVG species were expressed) or 37°C. For ER release and TGN accumulation, cells were shifted to 20°C for 2 h in the presence of 100 µg/ml cycloheximide (MP Biomedicals, Solon, OH). We used 3 µM rapamycin (LC Laboratories, Woburn, MA) when CAD proteins were involved. For post-TGN time points, cells were shifted to 32 or 37°C in the presence of rapamycin (for CAD cargo).

Cell fractionation

Cells were scraped in a homogenization buffer based on a Golgi isolation protocol geared toward preservation of peripheral membrane proteins (Fath *et al.*, 1997; 20 mM 4-(2-hydroxyethyl)-1-piperazineethanesulfonic acid [pH 6.8], 5 mM MgCl, 3 mM KCl, and 0.25 M sucrose supplemented with protease and phosphatase inhibitors [2 mM 4-(2-aminoethyl)benzenesulfonyl fluoride [alternatively, 1 mM benzamidine], 10 µg/ml leupeptin, 10 µg/ml pepstatin, 10 µg/ml antipain, 2 mM orthovanadate, 10 mM glycerophosphate, 5 mM Na pyrophosphate, 0.5 µM okadaic acid]) and disrupted by nitrogen cavitation, and the postnuclear supernatant was aliquoted, snap frozen, and stored at −80°C. Before processing of samples for immunofluorescence or EM, the postnuclear fractions were thawed, 0.22-µm-filtered bovine serum albumin (BSA) was added to a final concentration of 0.05%, and the fractions were sonicated by a 5-s pulse using a 3-mm stepped microtip (Sonics and Materials, Newtown, CT) and a 250-W analogue sonifier (Branson-Emerson, Danbury, CT) set to 30% power.

General immunofluorescence

For surface immunofluorescence, primary antibodies against cargo ectodomains were applied to both top and bottom sides of the filter membrane for 1.5 h at 4°C in bicarbonate-free DMEM supplemented with 10% fetal bovine serum (FBS) and 1% BSA before fixation in 2% paraformaldehyde (PFA) at 4°C. Otherwise, PFA fixation was at room temperature, and cells were permeabilized in 0.2% Triton X-100 and blocked in 1% BSA/10% FBS in phosphate-buffered saline. The following primary antibodies were used: giantin (G1/133; Enzo Life Sciences, Farmingdale, NY), GM 130 (clone 35; BD Biosciences, San Jose, CA), calnexin (TO-5, Sigma-Aldrich, St. Louis, MO; pAB, Enzo Life Sciences), VSVG cytoplasmic domain (P4D5; hybridoma from E. Rodriguez-Boulan, Weill Cornell Medical College, New York, NY), VSVG ectodomain (α5F; hybridoma from E. Rodriguez-Boulan, Cornell Medical College), EEA1 (BD Biosciences), CD26 (OX-61; Bio-Rad, Hercules, CA), Gp135 (3F21D8; from G. Ojakian, SUNY, Downstate Medical Center, New York, NY), NTRp75 cytoplasmic tail (from Moses Chao, New York University, New York, NY), NTRp75 ectodomain (MA20.4 hybridoma from E. Rodriguez-Boulan), and ZO1 (R26.4C; generated by D. Goodenough, distributed by the Developmental Studies Hybridoma Bank, University of Iowa, Iowa City, IA). Cells were imaged with a Leica SP5 microscope using an HCS Apo CS 63.0×/1.40 NA oil objective. Images used for establishing association between cargo and the Golgi markers had a pixel size of 141 nm.

Immunofluorescence of membrane fractions

Sonicated membrane fractions were applied on degreased air-dried coverslips and fixed with fixative buffer (2.5% PFA in fractionation buffer) at room temperature for 10 min. Fractions were washed and blocked in blocking buffer for 5 min. Antibodies were placed in blocking buffer and centrifuged briefly at 135,000 rpm. Primary antibodies (including TMR-Star coupled SNAP ligand; New England Biolabs, Ipswich, MA) were incubated on the samples for 15 min, followed by 3× washes for a total of 10 min in fractionation buffer. Secondary antibodies (Alexa Fluor 488 and 647, Jackson Immunoresearch, West Grove, PA; CY3, Molecular Probes) were incubated on the samples for 15 min, followed by the same washing step. Samples were postfixed in fixative buffer for 5 min, washed 1× briefly, and mounted with Mowiol on degreased, air-dried glass slides. Samples were imaged on a Zeiss Axiovert microscope equipped with a Hamamatsu Orca-R^2 cooled digital CCD camera using 1 × 1 binning (pixel size, 65 nm), 12-bit pixel depth, and a Zeiss Plan-Apochromat 100×/1.4 NA oil objective.

Correlated fluorescence and scanning electron microscopy

Cell fractions were fixed and stained on glass coverslips imprinted with three fiduciary markers. Samples were imaged using a Zeiss AxioObserver microscope equipped with AxioVision software with "shuttle & find" to mark fraction locations. After fluorescence imaging, samples were fixed with 2.5% glutaraldehyde, dehydrated in ethanol, critical point dried (Tousimis Samdri 790), and coated with chromium (EMS 150T-ES). The same cell fractions were automatically located in the Zeiss Supra 40 field emission scanning electron microscope (SEM) and imaged with a secondary electron detector. Fluorescence and SEM images were correlated with Zeiss AxioVision.

Algorithm for fluorescence peak selection

Fluorescence peaks detected by the CCD were analyzed based on their intensity and the shape of their pixel distributions. Intensity mapping transformation using the Redist module for the ImageMagick Suite was applied to redistribute the intensity histogram of each image to fit a Gaussian curve (in gray scale) to lower noise from low-intensity pixel values that affect correlative measurements. The Gaussian distribution was based on the cumulative histogram of each image's intensities, and the same Gaussian fitting parameters were applied to each image. The ImageMagick Suite is available free of charge under a GPLv3 license from ImageMagick Studios, LLC (www.imagemagick.org/). The Redist module is a copyright of Fred Weinhaus and is available free of charge for noncommercial use and is also subject to the ImageMagick Studios, LLC license (www.fmwconcepts.com/imagemagick/redist/). Fluorescence peaks from the redistributed images were then processed with TGNPeakMaster module. TGNPeakMaster fit a Gaussian along *x*- and *y*-axes over each localized fluorescence cluster of minimum size of 2 pixels. The circularity of each tentative peak was assessed as the difference in *x* and *y* Gaussian widths at half-maxima, and the Gaussian fit was further assessed by fitting to the minimum and maximum threshold values (Supplemental Figure S4). Thus peaks that were either noncircular or resulted in poor Gaussian fit due to irregular, low, or saturating intensities were discarded from the analysis (Supplemental Figure S5). Intensity values for all peaks that passed the Gaussian fitting step were recorded, and peaks with overlap of >15% were reported as colocalized. A "raw" Pearson correlation coefficient was obtained by plotting the intensities of the colocalized, calnexin-negative peaks, and a "raw" relative colocalized and single fraction abundance was quantified for each cargo. Differences in centroid coordinates between peaks in different channels were assessed to make sure that pixel shift between channels was not contributing to colocalization readout.

Algorithm for cell-based correction of membrane fraction data

Correlative data obtained from membrane fractions in the TGNPeakMaster analysis were corrected for the differences in expression observed in cells sampled just before fractionation. Coverslips placed along the edge of the plate of cells used in the fractionation experiments were incubated on the plate from the time of plating and removed and fixed before homogenization. The coverslips were processed for immunofluorescence of cargo and costained with the Golgi marker giantin (except for mRFP-ST–expressing cells, which had a stably expressed Golgi marker). Using ImageJ 1.49 (National Institutes of Health, Bethesda, MD), confocal stacks of 177 μm × 177 μm fields of view of the cells were summed, and a mask of the Golgi was made by thresholding the giantin or mRFP-ST channel. The mask was applied over the summed stacks of the two cargo channels after they were background corrected with a linear median value subtraction, and the resulting images were processed by JACOP plug-in (Bolte and Cordelieres, 2006) to obtain Pearson and Manders coefficients for the two cargo proteins. An average of several Pearson measurements was used to backcorrect the Pearson correlation measured for the membrane fractions processed by TGNPeakMaster, and an average of several Manders coefficients was used to backcorrect the relative number of colocalized versus single peaks.

Statistical testing

In addition to measuring Pearson correlation and relative colocalized fractions and further obtaining correlative indices corrected by the expression differences in the cells, we subjected distribution data for colocalized peaks from each cargo pair and time point obtained picked by TGNPeakMaster to bootstrap statistical analysis with 2000 random sampling iterations and a Sidak correction of α to account for multiple comparisons, resulting in correlation confidence interval comparison across all cargo pairs and time points. To characterize the relationship between the statistical parameters used to describe cargo relationships, we compared raw Pearson correlations, corrected correlation indices, and relative colocalized fractions by linear regression for the 28 samples used in the study (GraphPad Prism 6.0; GraphPad Software, La Jolla, CA).

ACKNOWLEDGMENTS

We acknowledge Geoffrey S. Perumal and Frank P. Macaluso at the Analytical Imaging Facility at Albert Einstein College of Medicine for the correlative light and electron microscopy imaging. We are grateful to John Murray at Einstein College of Medicine for advice on vesicle immunofluorescence. We thank K. Simons (Max Planck Institute for Developmental Biology, Dresden, Germany), O. Weisz (University of Pittsburgh Medical School, Pittsburgh, PA), and E. Rodriguez-Boulan (Weill Cornell Medical College, New York, NY) for providing cDNAs and hybridoma for this study. The work was supported by National Institutes of Health Grant RO1 DK064842 to A.M.

REFERENCES

Ang AL, Taguchi T, Francis S, Folsch H, Murrells LJ, Pypaert M, Warren G, Mellman I (2004). Recycling endosomes can serve as intermediates during transport from the Golgi to the plasma membrane of MDCK cells. J Cell Biol 167, 531–543.

Bolte S, Cordelieres FP (2006). A guided tour into subcellular colocalization analysis in light microscopy. J Microsc 224, 213–232.

Cramm-Behrens CI, Dienst M, Jacob R (2008). Apical cargo traverses endosomal compartments on the passage to the cell surface. Traffic 9, 2206–2220.
Cresawn KO, Potter BA, Oztan A, Guerriero CJ, Ihrke G, Goldenring JR, Apodaca G, Weisz OA (2007). Differential involvement of endocytic compartments in the biosynthetic traffic of apical proteins. EMBO J 26, 3737–3748.
Delacour D, Koch A, Jacob R (2009). The role of galectins in protein trafficking. Traffic 10, 1405–1413.
De Matteis MA, Luini A (2008). Exiting the Golgi complex. Nat Rev Mol Cell Biol 9, 273–284.
Falck-Pedersen E (1998). Use and application of adenovirus expression vectors. In: Cells. A Laboratory Manual, Vol. 2: Light Microscopy of Cell Structure, ed. DL Spector, RD Goldman, and LD Leinwand, Cold Spring Harbor, NY: Cold Spring Harbor Laboratory Press, 1–28.
Fath KR, Trimbur GM, Burgess DR (1997). Molecular motors and a spectrin matrix associate with Golgi membranes in vitro. J Cell Biol 139, 1169–1181.
Folsch H, Mattila PE, Weisz OA (2009). Taking the scenic route: biosynthetic traffic to the plasma membrane in polarized epithelial cells. Traffic 10, 972–981.
Glick BS, Luini A (2011). Models for Golgi traffic: a critical assessment. Cold Spring Harb Perspect Biol 3, a005215.
Gravotta D, Carvajal-Gonzalez JM, Mattera R, Deborde S, Banfelder JR, Bonifacino JS, Rodriguez-Boulan E (2012). The clathrin adaptor AP-1A mediates basolateral polarity. Dev Cell 22, 811–823.
Griffiths G, Pfeiffer S, Simons K, Matlin K (1985). Exit of newly synthesized membrane proteins from the trans cisterna of the Golgi complex to the plasma membrane. J Cell Biol 101, 949–964.
Griffiths G, Simons K (1986). The trans Golgi network: sorting at the exit site of the Golgi complex. Science 234, 438–443.
Guo X, Mattera R, Ren X, Chen Y, Retamal C, Gonzalez A, Bonifacino JS (2013). The adaptor protein-1 mu1B subunit expands the repertoire of basolateral sorting signal recognition in epithelial cells. Dev Cell 27, 353–366.
He TC, Zhou S, da Costa LT, Yu J, Kinzler KW, Vogelstein B (1998). A simplified system for generating recombinant adenoviruses. Proc Natl Acad Sci USA 95, 2509–2514.
Jacob R, Naim HY (2001). Apical membrane proteins are transported in distinct vesicular carriers. Curr Biol 11, 1444–1450.
Keller P, Toomre D, Diaz E, White J, Simons K (2001). Multicolour imaging of post-Golgi sorting and trafficking in live cells. Nat Cell Biol 3, 140–149.
Kreis TE, Lodish HF (1986). Oligomerization is essential for transport of vesicular stomatitis viral glycoprotein to the cell surface. Cell 46, 929–937.
Ladinsky MS, Kremer JR, Furcinitti PS, McIntosh JR, Howell KE (1994). HVEM tomography of the trans-Golgi network: structural insights and identification of a lace-like vesicle coat. J Cell Biol 127, 29–38.
Ladinsky MS, Mastronarde DN, McIntosh JR, Howell KE, Staehelin LA (1999). Golgi structure in three dimensions: functional insights from the normal rat kidney cell. J Cell Biol 144, 1135–1149.
Ladinsky MS, Wu CC, McIntosh S, McIntosh JR, Howell KE (2002). Structure of the Golgi and distribution of reporter molecules at 20 degrees C reveals the complexity of the exit compartments. Mol Biol Cell 13, 2810–2825.
Matlin KS, Simons K (1983). Reduced temperature prevents transfer of a membrane glycoprotein to the cell surface but does not prevent terminal glycosylation. Cell 34, 233–243.
Odorizzi G, Pearse A, Domingo D, Trowbridge IS, Hopkins CR (1996). Apical and basolateral endosomes of MDCK cells are interconnected and contain a polarized sorting mechanism. J Cell Biol 135, 139–152.
Patterson GH, Hirschberg K, Polishchuk RS, Gerlich D, Phair RD, Lippincott-Schwartz J (2008). Transport through the Golgi apparatus by rapid partitioning within a two-phase membrane system. Cell 133, 1055–1067.
Polishchuk RS, Polishchuk EV, Marra P, Alberti S, Buccione R, Luini A, Mironov AA (2000). Correlative light-electron microscopy reveals the tubular-saccular ultrastructure of carriers operating between Golgi apparatus and plasma membrane. J Cell Biol 148, 45–58.
Rabouille C, Hui N, Hunte F, Kieckbusch R, Berger EG, Warren G, Nilsson T (1995). Mapping the distribution of Golgi enzymes involved in the construction of complex oligosaccharides. J Cell Sci 108, 1617–1627.
Ren M, Xu G, Zeng J, De Lemos-Chiarandini C, Adesnik M, Sabatini DD (1998). Hydrolysis of GTP on rab11 is required for the direct delivery of transferrin from the pericentriolar recycling compartment to the cell surface but not from sorting endosomes. Proc Natl Acad Sci USA 95, 6187–6192.
Reyes FC, Buono R, Otegui MS (2011). Plant endosomal trafficking pathways. Curr Opin Plant Biol 14, 666–673.
Rindler MJ, Ivanov IE, Plesken H, Rodriguez-Boulan E, Sabatini DD (1984). Viral glycoproteins destined for apical or basolateral plasma membrane domains traverse the same Golgi apparatus during their intracellular transport in doubly infected Madin-Darby canine kidney cells. J Cell Biol 98, 1304–1319.
Rindler MJ, Ivanov IE, Plesken H, Sabatini DD (1985). Polarized delivery of viral glycoproteins to the apical and basolateral plasma membranes of Madin-Darby canine kidney cells infected with temperature-sensitive viruses. J Cell Biol 100, 136–151.
Rivera VM, Wang X, Wardwell S, Courage NL, Volchuk A, Keenan T, Holt DA, Gilman M, Orci L, Cerasoli F Jr, Rothman JE, Clackson T (2000). Regulation of protein secretion through controlled aggregation in the endoplasmic reticulum. Science 287, 826–830.
Roth J, Taatjes DJ, Lucocq JM, Weinstein J, Paulson JC (1985). Demonstration of an extensive trans-tubular network continuous with the Golgi apparatus stack that may function in glycosylation. Cell 43, 287–295.
Salvarezza SB, Deborde S, Schreiner R, Campagne F, Kessels MM, Qualmann B, Caceres A, Kreitzer G, Rodriguez-Boulan E (2009). LIM kinase 1 and cofilin regulate actin filament population required for dynamin-dependent apical carrier fission from the trans-Golgi network. Mol Biol Cell 20, 438–451.
Thompson A, Nessler R, Wisco D, Anderson E, Winckler B, Sheff D (2007). Recycling endosomes of polarized epithelial cells actively sort apical and basolateral cargos into separate subdomains. Mol Biol Cell 18, 2687–2697.
Toomre D, Keller P, White J, Olivo JC, Simons K (1999). Dual-color visualization of trans-Golgi network to plasma membrane traffic along microtubules in living cells. J Cell Sci 112, 21–33.
Treyer A, Musch A (2013). Hepatocyte polarity. Compr Physiol 3, 243–287.
Wandinger-Ness A, Bennett MK, Antony C, Simons K (1990). Distinct transport vesicles mediate the delivery of plasma membrane proteins to the apical and basolateral domains of MDCK cells. J Cell Biol 111, 987–1000.
Wang E, Brown PS, Aroeti B, Chapin SJ, Mostov KE, Dunn KW (2000). Apical and basolateral endocytic pathways of MDCK cells meet in acidic common endosomes distinct from a nearly-neutral apical recycling endosome. Traffic 1, 480–493.
Wang E, Pennington JG, Goldenring JR, Hunziker W, Dunn KW (2001). Brefeldin A rapidly disrupts plasma membrane polarity by blocking polar sorting in common endosomes of MDCK cells. J Cell Sci 114, 3309–3321.
Wehland J, Willingham MC, Gallo MG, Pastan I (1982). The morphologic pathway of exocytosis of the vesicular stomatitis virus G protein in cultured fibroblasts. Cell 28, 831–841.
Weisz OA, Machamer CE, Hubbard AL (1992). Rat liver dipeptidylpeptidase IV contains competing apical and basolateral targeting information. J Biol Chem 267, 22282–22288.
Weisz OA, Rodriguez-Boulan E (2009). Apical trafficking in epithelial cells: signals, clusters and motors. J Cell Sci 122, 4253–4266.
Wilcke M, Johannes L, Galli T, Mayau V, Goud B, Salamero J (2000). Rab11 regulates the compartmentalization of early endosomes required for efficient transport from early endosomes to the trans-golgi network. J Cell Biol 151, 1207–1220.